

Energy Response of the X-ray Imaging Spectrometer (XIS) on Suzaku

Hironori Matsumoto, Hiroshi Nakajima, Hiroya Yamaguchi, Takeshi G. Tsuru, Katsuji Koyama^a, Kiyoshi Hayashida, Ken'ichi Torii, Masaaki Namiki, Hiroshi Tsunemi^b, Hiroshi Murakami, Masanobu Ozaki, Tadayasu Dotani^c, Beverly LaMarr, Steven E. Kissel, Mark W. Bautz^d

^aDepartment of Physics, Graduate School of Science, Kyoto University, Kyoto 606-8502, Japan;

^bDepartment of Earth and Space Science, Osaka University, Osaka 560-0043, Japan

^cInstitute of Space and Astronomical Science/Japan Aerospace Exploration Agency, Kanagawa 229-8510, Japan

^dKavli Institute for Astrophysics and Space Research, Massachusetts Institute of Technology, Cambridge, MA 02139-4307, USA

ABSTRACT

The X-ray Imaging Spectrometer on the Suzaku satellite consists three front-illuminated (FI) and one back-illuminated (BI) CCD cameras. Using ground calibration data taken at Kyoto University and Osaka University, we obtained the energy response of the XIS, which consists of at least six components: 1. a main peak, 2. a sub peak, 3. a triangle component, 4. a Si escape, 5. a Si line, and 6. a constant component. The relation between the energy and the pulse height was also estimated, which is called as a gain. The relation cannot be represented with a single linear function. Then we divided the gain into two parts at the Si edge (1.839 keV) and each part can be described with a single linear function. Thus there is a discontinuity at 1.839 keV in the XIS gain. We have monitored the variation of the gain and energy resolution in orbit by observing the calibration source of ⁵⁵Fe illuminating two corners of each CCD.

Keywords: Suzaku satellite, X-ray CCD, energy response

1. INTRODUCTION

Suzaku is the fifth Japanese X-ray astronomical satellite, which was launched on July 10, 2005 from Uchinoura Space Center at Kagoshima, Japan. Suzaku covers the energy range 0.2 - 700 keV with the three instruments: an X-ray micro-calorimeter (X-Ray Spectrometer, or XRS), a hard X-ray detector, or HXD, and four X-ray CCDs (the X-ray Imaging Spectrometers, or XISs).

The XRS has an extremely high energy resolution (FWHM \sim 6 eV at 5.9 keV) in the 0.3 - 12 keV band.¹ However, the XRS has lost its function because of the loss of a helium cryogen. The HXD consists of phoswich scintillation counters (GSO/BGO) and silicon PIN diodes and has a sensitivity in the 10 - 600 keV band.²

The XIS consists of four X-ray CCD cameras (XIS0-3) at the foci of four X-Ray Telescopes (XRT). Only the XIS has an imaging capability with a moderate energy resolution, and is complementary to the other detectors. Figure 1 shows the schematic view of an XIS sensor. Each CCD sensor has a single CCD chip, which is a MOS-type three-phase CCD operated in the frame transfer mode. The exposure area of the CCD consists of 1024 \times 1024 pixels. Since the pixel size is 24 μ m \times 24 μ m, the exposure area has a size of 25mm \times 25mm. The exposure area covers an 18' \times 18' region on the sky combined with the XRT. There are four readout gates for each CCD chip. Each gate reads out 256 \times 1024 pixels, which is called as a segment (marked A, B, C, and D in Fig. 1). There are no physical boundaries between the segments, but calibrations are done for each segment because characteristics such as gain, energy resolution, readout noise, and quantum efficiency are slightly different between the segments, even if they are on the same CCD chip.

Further author information: (Send correspondence to Hironori Matsumoto)
Hironori Matsumoto: E-mail: matumoto@cr.scphys.kyoto-u.ac.jp, FAX: +81-75-753-3799

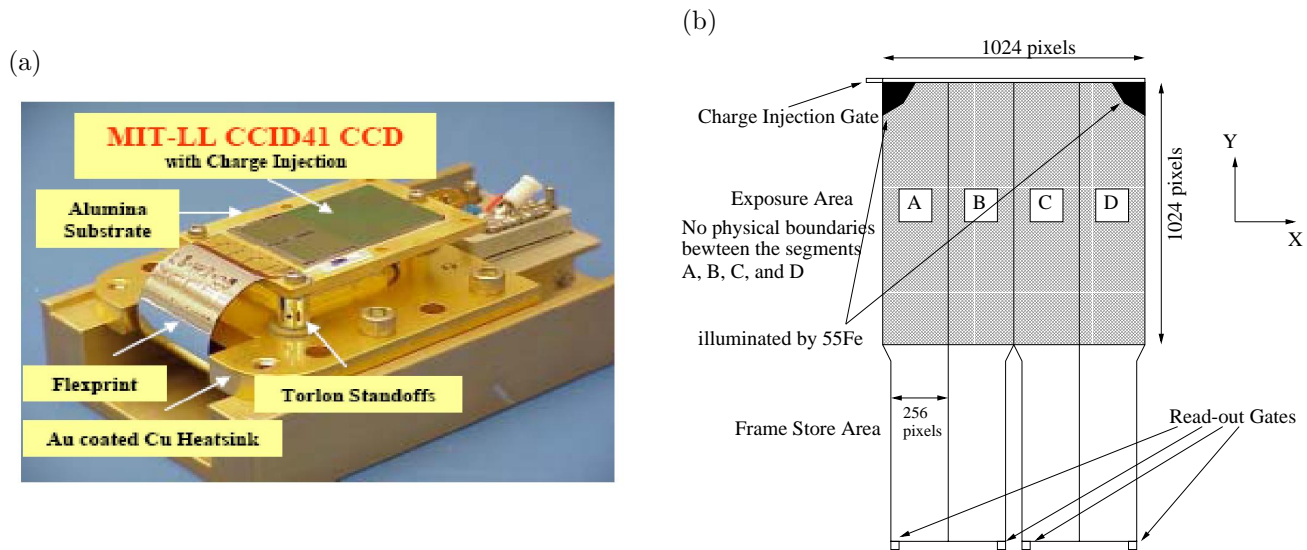


Figure 1. Photo (a) and schematic view (b) of an XIS sensor. Each XIS consists of a single CCD chip with an imaging area of 1024×1024 pixels. Each pixel size in the imaging area is $24\mu\text{m} \times 24\mu\text{m}$. There are four readout gates for one XIS sensor, and each of them reads out 256 columns, which is 1/4 of the imaging area. The 1/4 regions are referred to as segments A, B, C, and D. There is a charge injection gate on top of the imaging area.

One of the four XIS sensors (XIS1) utilizes a back-side illuminated (BI) CCD, while the other three (XIS0, 2, and 3) are equipped with front-side illuminated (FI) CCDs. The FI CCD detects X-rays coming through the front surface of the CCD where there is a gate layer consists mainly of Si and SiO_2 . On the other hand, X-rays enter the BI CCD through the back side where there is no gate layer. The BI CCD is thus more sensitive to soft X-rays than the FI CCD. However, because the BI CCD needs to be thinned to remove an undepletion layer completely, the depletion layer of the BI CCD is thinner than the FI CCD. Thus the FI CCD has high quantum efficiency at high energies.

Figures 2 and 3 are examples of X-ray spectra of celestial objects obtained with the XIS. The spectra of SNR 0102-72.3 tells us that the energy resolution of the BI CCD is almost comparable to the FI CCD. It is rather impressive that both the FI and BI CCDs can resolve the iron line complex clearly into three lines at 6.4 keV (neutral Fe), 6.7 keV (Fe XXV), and 6.9 keV (Fe XXVI).

In this paper, we will describe the energy response of the XIS. Other characteristics of the XIS are reported in other papers in this volume.³⁻⁵ General information on the XIS is available in Ref. 6. Errors are estimated at the 90% confidence level.

2. ENERGY RESPONSE

Even if an incident X-ray beam is monochromatic, the pulse height (PH) distribution of the signals is not like the delta function. A map from the energy space of the incident photons to the detector PH space is called as an energy response of the detector. To construct the energy response, we had took XIS data by using the systems at Kyoto University⁷ and at Osaka University.⁸

Figures 4 and 5 show the PH distribution of the FI and BI CCDs to the ^{55}Fe X-rays (Mn $K\alpha$ 5.89 keV and Mn $K\beta$ 6.49 keV) and the characteristic X-rays of O $K\alpha$ (0.52 keV). In Fig. 4(a) and 5(a), we can see a main peak as well as a Si K escape peak and a Si $K\alpha$ line. The main peak cannot be fitted with a single Gaussian model, and it has a tail at the lower PH side. The tail becomes larger in the low energy response as shown in Fig. 4(b) and 5(b). The tail component requires the second Gaussian model, which is referred to as a “sub peak component”. In the case of the FI response, there is a “triangle component” in addition to the sub peak to describe the tail. Furthermore, we can see a “constant component” at the lower PH side of the main peak.

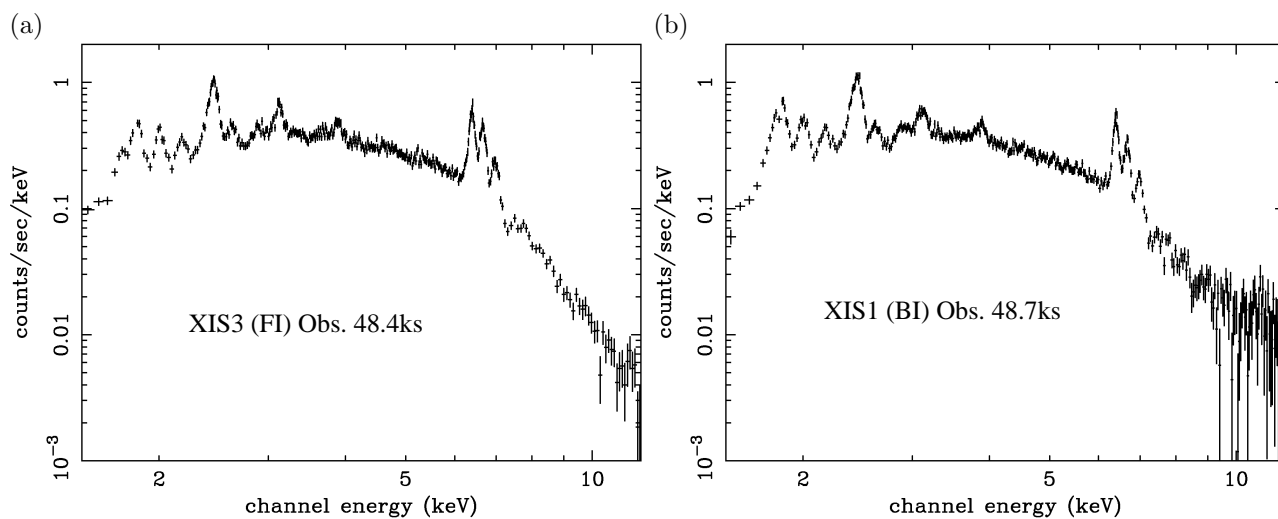


Figure 2. X-ray spectra of the Galactic center region obtained with (a) XIS3 (FI) and (b) XIS1 (BI).

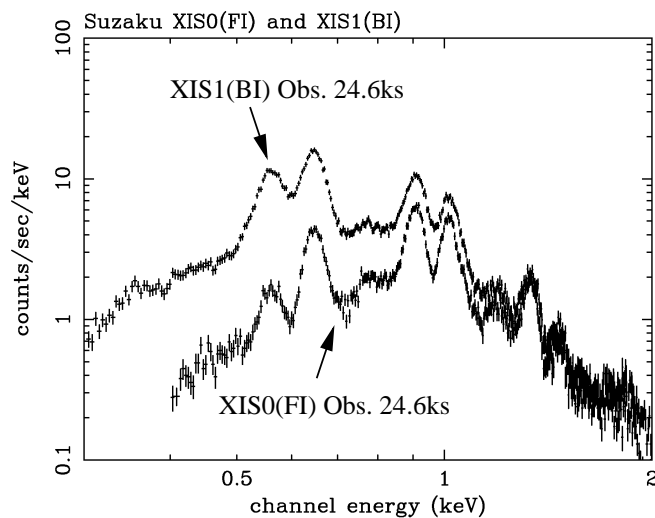


Figure 3. X-ray spectra of SNR 0102-72.3 obtained with XIS0 (FI) and XIS1 (BI).

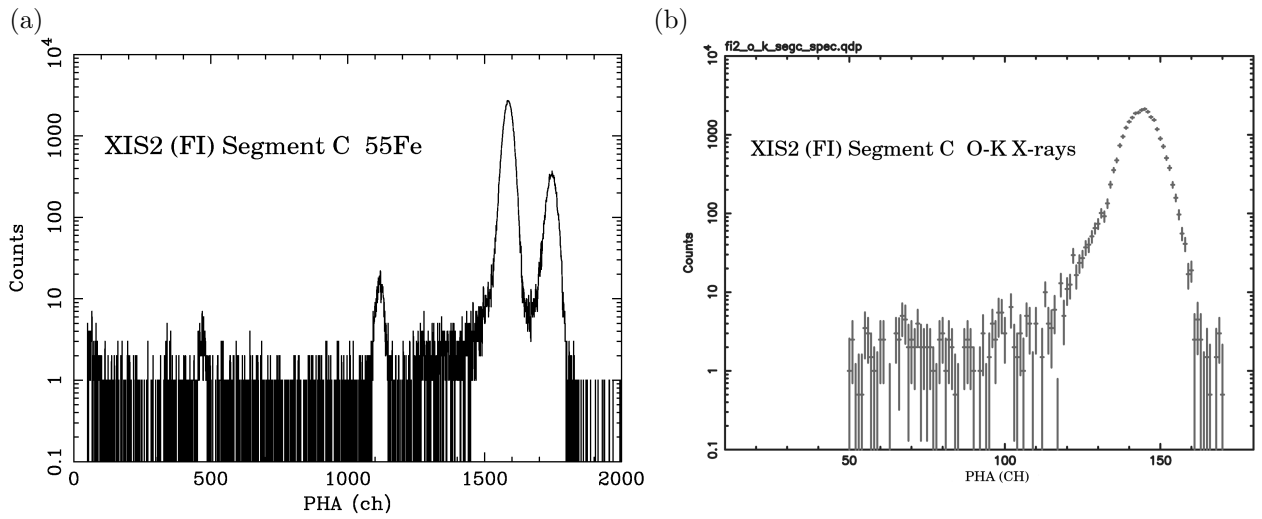


Figure 4. Pulse height distribution of the XIS2 (FI) segment C for monochromatic X-rays: (a) ^{55}Fe (the X-ray energies are 5.89 keV and 6.49 keV) and (b) the characteristic X-rays of O $K\alpha$ (0.52 keV).

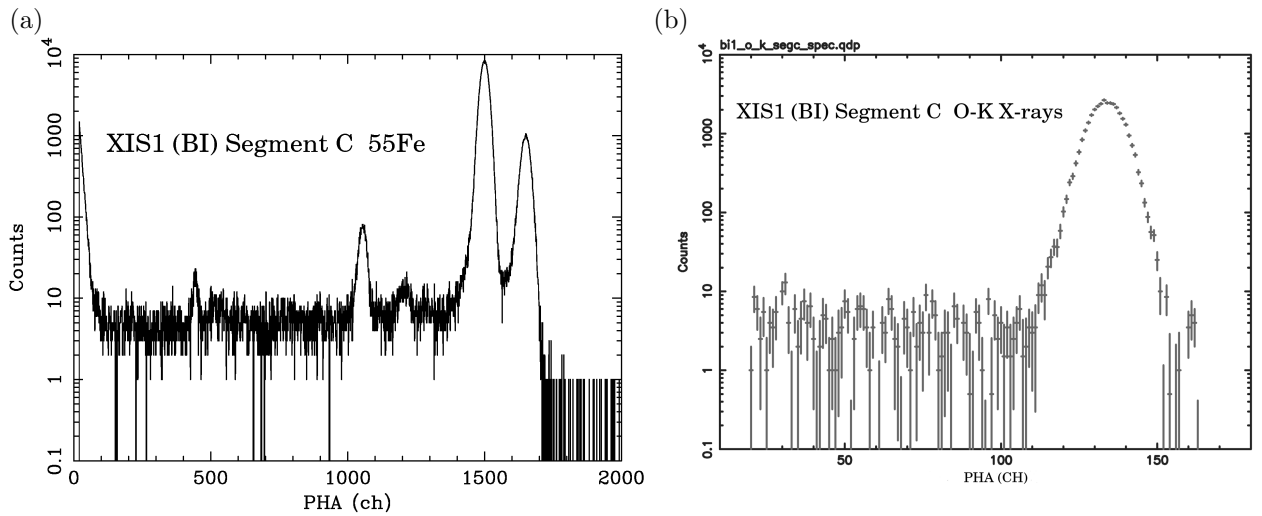


Figure 5. Pulse height distribution of the XIS1 (BI) segment C for monochromatic X-rays: (a) ^{55}Fe (5.89 keV and 6.49 keV) and (b) O $K\alpha$ line (0.52 keV).

In summary, the response of the XIS consists of at least six components as shown in Fig. 6. Physical interpretations of these components are following:

1. Main peak component

This component is described by a Gaussian model centered at a PH channel corresponds to the energy of an incident X-ray photon.

The X-ray photon is absorbed at the depletion layer of the CCDs and all electrons are collected as a signal.

2. Sub peak component

This component is a part of the “tail” component and is described by a Gaussian model slightly at a lower PH channel than the main peak component.

An X-ray photon is absorbed at the depletion layer, but electrons are split over a few pixels. Some of the pixels have a PH lower than the split threshold and are not counted as a signal.

3. Triangle component

This component also constitutes the “tail” of the main peak. We can see this component only in the FI response and there is no triangle component in the BI response.

An X-ray photon is absorbed at channel stops which serve to form pixel boundaries along the vertical direction (Y axis in Fig. 1). The channel stop is a P⁺-type Si layer and the density of acceptors is larger than the surrounding Si layer. Therefore a part of electrons generated in the channel stop is expected to be lost due to a recombination or a trap in the layer.

4. Si escape

This is expressed by a Gaussian model centered at the PH channel lower than the main peak by 1.74 keV which is the energy of the Si K α line.

After an X-ray photon is absorbed at the depletion layer, the fluorescent X-ray photon of Si is generated. The Si X-ray photon escapes from the pixel which absorbed the incident X-ray photon.

5. Si line

This is described by a Gaussian model centered at 1.74 keV. The fluorescent X-ray photon of Si is absorbed at a pixel far from the place where an incident X-ray photon was absorbed.

6. Constant component

An X-ray photon is absorbed at a place close to the boundary between the depletion layer and the insensitive layer. Then only a part of electrons can be collected as a signal.

3. GAIN AND ENERGY RESOLUTION

The relation of the center of the main peak component and the incident X-ray energy is called as a gain. We obtained the gain by fitting the PH distribution around the main peak with two Gaussian models (the main peak + the sub peak) for simplicity, which is shown in Fig. 7(a) and 8(a). The gain cannot be described with a single linear relation. This is probably because there is a sudden (but small) change in the mean energy for electron-hole creation (so-called the W value) at the energy of the Si edge (1.839keV). Then we divided the gain into two parts at 1.839 keV and fitted each part with a linear relation of $A * E + B$, where A and B is free parameters, and E is the energy. Thus there is a discontinuity at 1.839 keV in the gain of the XIS. In the case of the XIS1 (BI) segment C, the best-fit parameters are $A = 255.484 \pm 0.050$ and $B = -1.983 \pm 0.035$ for $E < 1.839$ keV, and $A = 255.182 \pm 0.017$ and $B = -2.494 \pm 0.093$ for $E \geq 1.839$ keV. For the case of the XIS2 (FI) segment C, the best-fit parameters are $A = 270.012 \pm 0.029$ and $B = 2.447 \pm 0.031$ for $E < 1.839$ keV, and $A = 268.232 \pm 0.010$ and $B = 9.353 \pm 0.052$ for $E \geq 1.839$ keV.

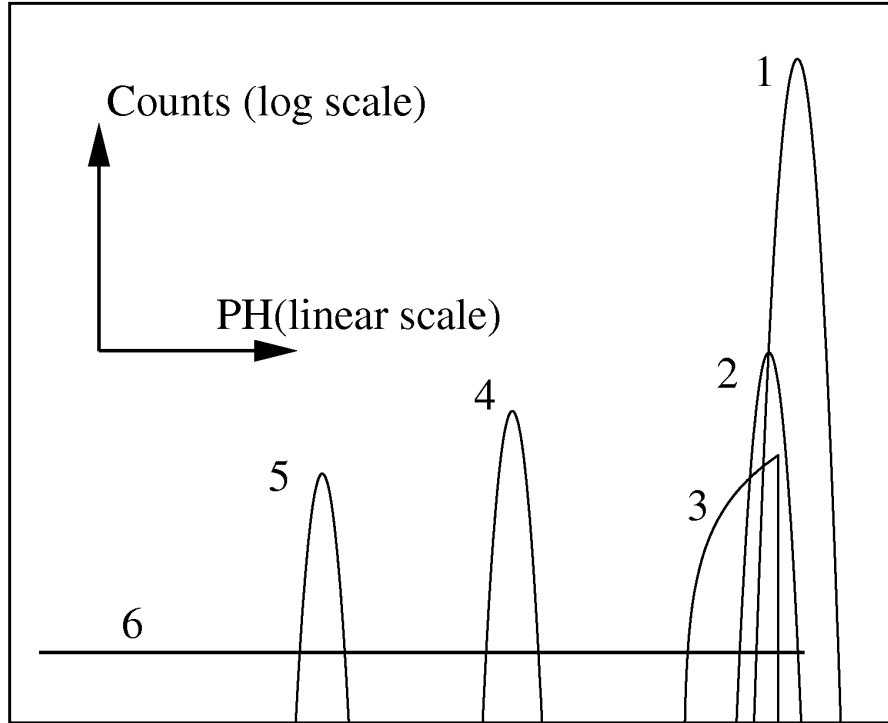


Figure 6. Schematic description of six components in the XIS response: 1. main peak, 2. sub peak, 3. triangle component, 4. Si escape, 5. Si $K\alpha$ line, and 6. constant component.

Figures 7(b) and 8(b) are the width of the main peak component as a function of the energy. The relation can be fitted with a function of $\sqrt{A \times E^2 + B \times E + C}$, where A , B , and C are free parameters. For the XIS1 (BI) segment C, the best-fit parameters are $A = -48.66 \pm 7.42$, $B = 3086.7 \pm 44.5$ and $C = 825.0 \pm 24.5$, while they are $A = 81.63 \pm 5.09$, $B = 2374.7 \pm 18.9$ and $C = 236.2 \pm 13.3$ in the case of the XIS2 (FI) segment C.

These results are based on data taken with the normal mode. Another clock mode for the XIS is the parallel-sum (P-sum) mode. In the P-sum mode, the pixel data from multiple rows are summed in the Y-direction on the CCD to enable fast readout.⁶ Since the clock is rather different, the gain and energy resolution of the P-sum mode can be different from those of the normal mode, which is currently under investigation.

4. TIME VARIATION OF THE GAIN AND RESOLUTION

The results shown in the previous sections are based on data taken during ground calibrations before the launch. Since the XIS have suffered radiation damage in a space environment, the charge transfer inefficiency (CTI) has increased since the launch. This causes the change of the gain and the degradation of the energy resolution. For on-orbit calibration, each sensor has two isotopes of $^{55}\text{Fe}^*$. They are located on the side wall of a housing and illuminate two corners of the imaging area far from the readout gates (Fig. 1). We have monitored the peak and width of the Mn $K\alpha$ line (Fig. 9). The center energy has gradually decreased since the launch. We estimate the CTI by using the data and do the CTI correction to all observational data, which are distributed to an observer. Figure 9(b) shows that the energy resolution has gradually degraded. We will take into account the degradation in making XIS response matrices in future, although the current XIS responses as of May 2006 have not been produced by considering it.

*There is another ^{55}Fe isotope attached to a sensor door. This source had illuminated the whole imaging area before the door opened. However few X-ray photons from the isotope enter the CCDs once the door opened.

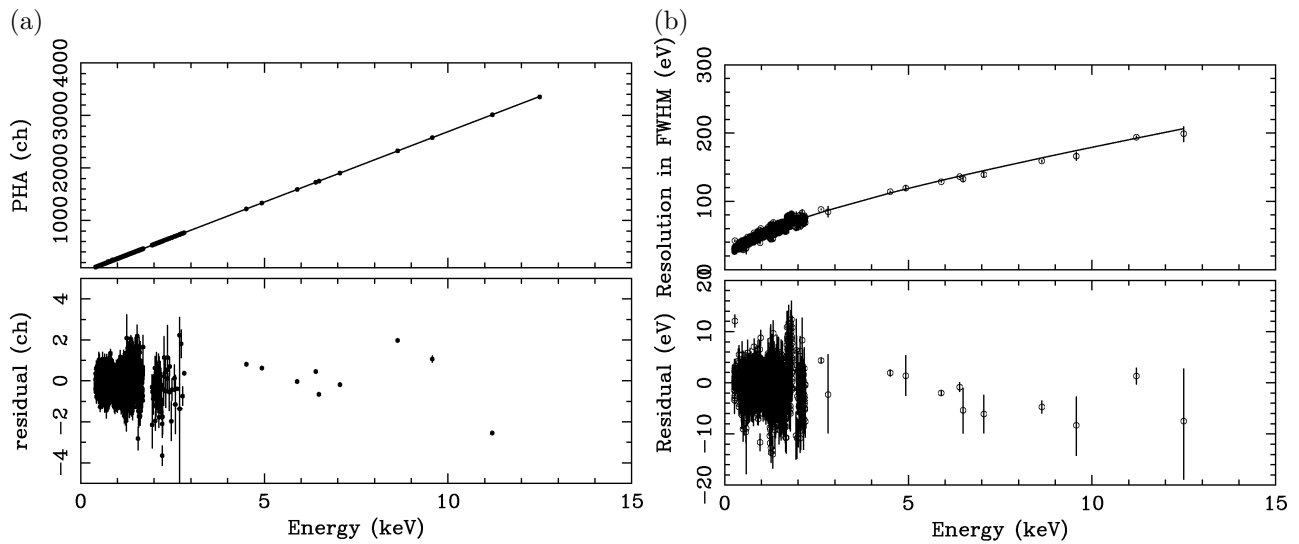


Figure 7. Gain (a) and energy resolution (b) of the XIS2 (FI) segment C as a function of the incident X-ray energy. The gain relation is divided into two parts at the energy of the Si edge (1.839 keV) and each part is fitted with a linear relation of $A \times E + B$, where A and B is free parameters, and E is the energy. Thus there is a discontinuity at 1.839 keV in the gain relation. The best-fit parameters are $A = 270.012 \pm 0.029$ and $B = 2.447 \pm 0.031$ for $E < 1.839$ keV, and $A = 268.232 \pm 0.010$ and $B = 9.353 \pm 0.052$ for $E \geq 1.839$ keV. The energy resolution is fitted with a function of $\sqrt{A \times E^2 + B \times E + C}$, where A , B , and C are free parameters. The best-fit parameters are $A = 81.63 \pm 5.09$, $B = 2374.7 \pm 18.9$ and $C = 236.2 \pm 13.3$.

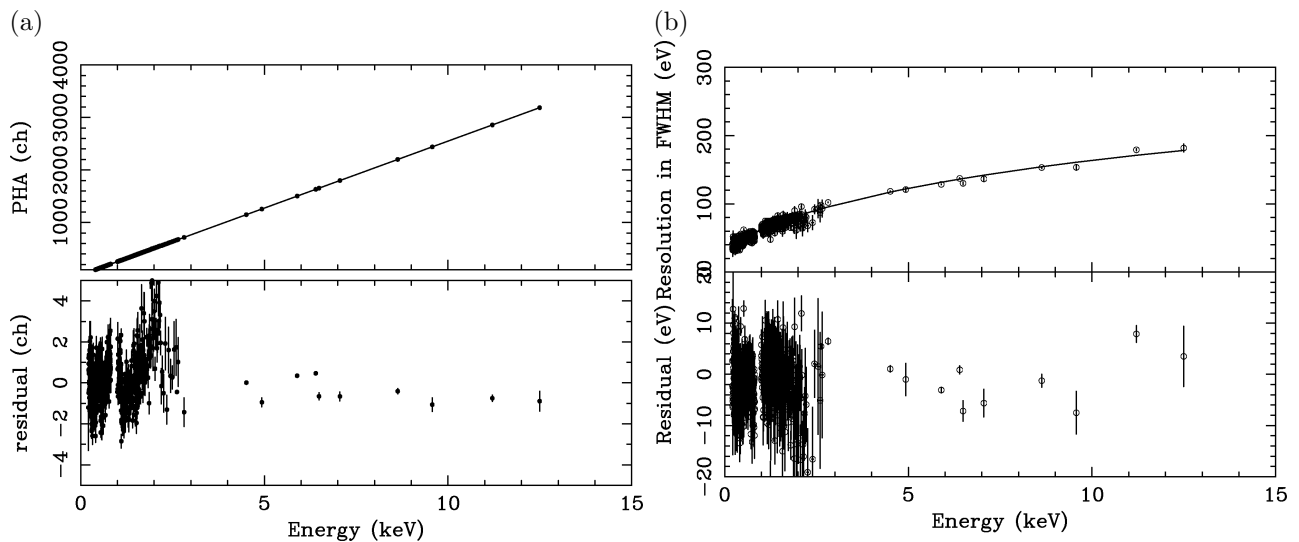


Figure 8. Same as Fig. 7 but for the XIS1 (BI). The best-fit parameters for the gain are $A = 255.484 \pm 0.050$ and $B = -1.983 \pm 0.035$ for $E < 1.839$ keV, and $A = 255.182 \pm 0.017$ and $B = -2.494 \pm 0.093$ for $E \geq 1.839$ keV. The best-fit parameters for the energy resolution are $A = -48.66 \pm 7.42$, $B = 3086.7 \pm 44.5$ and $C = 825.0 \pm 24.5$.

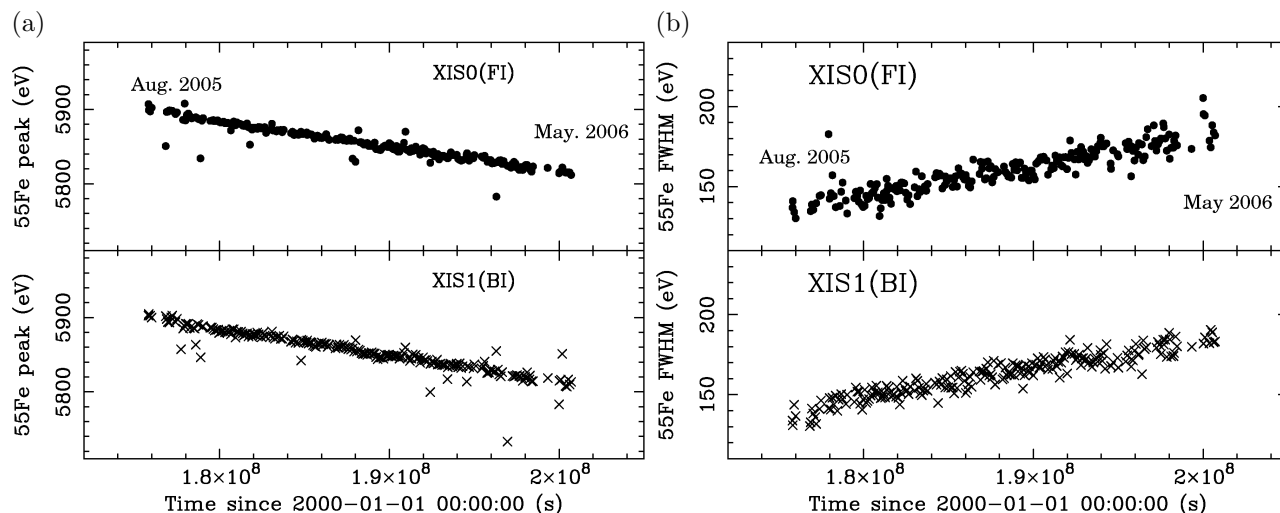


Figure 9. Center energy (a) and width in FWHM (b) of the Mn $K\alpha$ line from the calibration isotope of ^{55}Fe . Data of XIS0(FI) and XIS1(BI) are shown.

5. SUMMARY

We have reviewed the energy response of the XIS. The response to monochromatic X-rays consists of at least six components: 1. the main peak, 2. the sub peak, 3. the triangle component, 4. the Si escape, 5. the Si $K\alpha$ line, and 6. the constant component. We estimated the gain by using the center PH channel of the main peak, and the gain is not described with a single linear function. The gain can be divided into two parts at the Si edge energy (1.839 keV), and each of them can be expressed with a single linear function. Thus there is a discontinuity in the XIS gain at 1.839 keV. The change of the gain and the degradation of the energy resolution have been monitored by using the onboard calibration source (^{55}Fe) since the launch.

REFERENCES

1. K. Mitsuda et al., "XRS-2 - the High Resolution X-ray Spectrometer on Astro-E2", *New Century of X-ray Astronomy, ASP Conference Series*, H. Inoue and H. Kunieda eds., **251**, pp. 570-571, 2001
2. K. Makishima et al., "The HXD-II on Astro-E2: Another Challenge to the Hard X-ray Sky", *New Century of X-ray Astronomy, ASP Conference Series*, H. Inoue and H. Kunieda eds., **251**, pp. 564-565, 2001
3. K. Hayashida et al., "Orbital verification of the performance of Suzaku XIS" in *Proc. SPIE*, this volume, 2006
4. T. Miyauchi et al., "Quantum efficiencies of the XIS CCDs onboard Suzaku" in *Proc. SPIE*, this volume, 2006
5. H. Yamaguchi et al., "The background properties of Suzaku/XIS" in *Proc. SPIE*, this volume, 2006
6. H. Matsumoto et al. "X-ray imaging spectrometers (XIS) of Astro-E2", *Nuclear Instruments & Methods in Physics Research Section A*, **541**, 357-364, 2005
7. K. Hamaguchi et al. "X-ray CCD calibration system using fluorescent lines", *Nuclear Instruments & Methods in Physics Research Section A*, **450**, 360-364, 2000
8. K. Hayashida et al., "X-ray imaging spectrometers for Astro-E: ground calibration in the soft x-ray range" in *X-Ray Optics, Instruments, and Missions III*, J. E. Truemper and B. Aschenbach ed., *Proc. SPIE*, **4012**, pp. 123-136, 2000